A Novel Deformable Model for Medical US Image Segmentation

Michalis A. Savelonas[1], Dimitris E. Maroulis[1], Dimitris K. Iakovidis[1], Stavros A. Karkanis[2]

[1] University of Athens, Dept. of Informatics and Telecommunications, Panepistimiopolis, 15784 Ilisia, Greece
[2] Technological Educational Institute of Lamia, Dept. of Informatics and Computer Technology, 35100 Lamia, Greece
rtsimage@di.uoa.gr

Abstract. Medical ultrasound (US) images are characterized by inherent noise perturbations which introduce uncertainty in their interpretation even by experienced radiologists. In this paper we propose a novel deformable model for medical US image segmentation, which incorporates a combination of domain and boundary integrals for the alleviation of the noise effects. It can be applied as a diagnostic aid for the delineation of hypo-echoic regions, which in many cases are associated with pathological findings. The proposed model was experimentally evaluated using various types of medical US images. The results show that it leads to more accurate segmentation results whereas it converges faster than other relevant models.

1 Introduction

The inherent noise characteristics of medical ultrasound (US) images introduce uncertainty in their interpretation even by experienced radiologists. The application of image segmentation methods could enhance the efficiency and the effectiveness of screening by indicating regions of suspicious abnormal tissues based on explicit image features.

Medical US image segmentation methods that have been proposed in the literature include region growing [1-3], clustering [4], mathematical morphology [5], thresholding [6], wavelet analysis [7], support vector machines [8], genetic [9] and fuzzy [10] algorithms. The utilization of deformable models for medical US image segmentation has been gaining increasing interest as they provide a number of advantageous properties over other methods. A deformable model can be considered as a flexible surface deforming under the influence of external forces derived from image data and constraints preserving the consistency of a shape. It is self-adaptive, it allows for the construction of continuous, closed or open, curves without requiring edge-linking operations, and they are relatively noise insensitive because they involve integral operators which provide an inherent noise filtering mechanism [11].

Applications of deformable models in medical US image segmentation include the detection of hepatic tumors [11], the detection of lumen and media-adventitia border in sequential intravascular ultrasound frames [12], the evaluation of margins for malignant breast tumor excision through mammotomes [13], the automatic quantification of the ventricular function [14] and the determination of abnormal formations in prostate [15] and cardiac US images [16]. In most of these applications pathological findings are associated with hypo-echogenicity.

In this paper we propose a novel deformable model for medical US image segmentation which aims to the detection of hypo-echoic regions. It is derived as an application-specific extension of a state of the art model proposed in [17]. It incorporates modifications in the formulation of the original model that contribute to the reduction of the intensity inhomogeneity effects attributed to noise, tissue texture and calcifications. It is experimentally showed that the proposed model results in more accurate delineation of hypo-echoic regions in various US images whereas it converges faster.

The rest of this paper comprises of three sections. Section 2 describes the original [17] and the proposed novel medical US image segmentation method. Section 3 presents the experimental results obtained from the application of both methods on various medical US images. A summary of conclusions and future perspectives are apposed in the last section.

2 Methods

The proposed medical US image segmentation method is based on a novel deformable model derived from the model posed in [17]. It has the form of a minimization problem: Let Ω be a bounded open subset of R^2 and $\partial\Omega$ its boundary. We seek for $\inf F(c^+, c^-, C)$,

$$\begin{aligned} F(c^+, c^-, C) = {} & \mu \cdot Length(C) \\ & + \lambda^+ \int_{inside(C)} |\, u_0(x,y) - c^+ \,|^2 \, dxdy \\ & + \lambda^- \int_{outside(C)} |\, u_0(x,y) - c^- \,|^2 \, dxdy \end{aligned} \tag{1}$$

where $u_0 : \Omega \to R$ is the input image, $C(s) : [0,1] \to R^2$ a piecewise parameterized curve, c^+ and c^- represent average values of u_0 inside and outside the curve and the parameters $\mu > 0$ and $\lambda^+, \lambda^- > 0$ are weights for the regularizing term and the fitting terms, respectively. This problem is a special case of the minimal partition problem, for which the existence of minimizers has been proved in [18] for u_0 continuous on Ω and in [19] for more general data. As in the minimum energy problem, the minimizer corresponds to the "equilibrium" of the regularizing and fitting terms that force the contour to stop.

The curve $C \subset \Omega$ is represented by the zero level set of a Lipschitz function $\phi : \Omega \to R$, such that

$$
\begin{aligned}
&C = \{(x,y) \in \Omega : \phi(x,y) = 0\}, \\
&inside(C) = \{(x,y) \in \Omega : \phi(x,y) > 0\}, \\
&outside(C) = \{(x,y) \in \phi(x,y) < 0\}
\end{aligned} \tag{2}
$$

Using the one-dimensional Dirac measure δ and the Heaviside function H, which are defined respectively by

$$
\delta(z) = \frac{d}{dz} H(z), \quad H(z) = \begin{cases} 1, & if\ z \geq 0 \\ 0, & if\ z < 0 \end{cases} \tag{3}
$$

where $z \in R$. The original deformable model as described in [17] utilizes c^+ and c^- expressed by the following equations:

$$
c^+(\phi) = \frac{\int_\Omega u_0(x,y) H(\phi(x,y)) dxdy}{\int_\Omega H(\phi(x,y)) dxdy} \tag{4}
$$

$$
c^-(\phi) = \frac{\int_\Omega u_0(x,y)(1 - H(\phi(x,y))) dxdy}{\int_\Omega (1 - H(\phi(x,y))) dxdy} \tag{5}
$$

The intensity inhomogeneity present in the US images affects c^- which corresponds to the average background intensity. The proposed model introduces a new c^- which is calculated as the average of the remaining background when inhomogeneity regions are excluded.

We define $\Delta(x,y)$ such as

$$
\Delta(x,y) = H(\phi(x,y) - a) - H(\phi(x,y)) \tag{6}
$$

where α is a positive constant. Moreover, we assume that the initial contour as traced by ϕ_0 corresponds to a region of interest within the interior of the thyroid gland and we employ $H(\phi_0)$ to restrict the calculation of c^+ and c^- over this region. Equations (4) and (5) are reformulated as follows

$$
c^+(\phi) = \frac{\int_\Omega u_0(x,y) H(\phi(x,y)) H(\phi_0(x,y)) dxdy}{\int_\Omega H(\phi(x,y)) H(\phi_0(x,y)) dxdy} \tag{7}
$$

$$
c^-(\phi) = \frac{\int_\Omega u_0(x,y)(1 - H(\phi(x,y))) H(\phi_0(x,y)) \Delta(x,y) dxdy}{\int_\Omega (1 - H(\phi(x,y))) H(\phi_0(x,y)) \Delta(x,y) dxdy} \tag{8}
$$

Equation (8) imposes that a point $(x, y) \in \Omega$ is not included in the calculation of c^- if $\Delta(x, y) = 0$. These points correspond to inhomogeneities within the region of interest due to the fact that the intensity inhomogeneities cause abrupt changes of ϕ which result in $H(\phi(x, y) - a) = H(\phi(x, y)) = 1$.

By keeping c^+ and c^- fixed, and minimizing F with respect to ϕ, the associated Euler-Langrange equation for ϕ is deduced. For this purpose, slightly regularized versions of H and δ are considered. The regularized Heaviside function H_ε is derived from

$$H_\varepsilon = \frac{1}{2} \cdot (1 + \frac{2}{\pi} \arctan(\frac{z}{\varepsilon})) \tag{9}$$

whereas the corresponding regularized delta function δ_ε is derived from $\delta_\varepsilon = dH_\varepsilon / dz$. As $\varepsilon \to 0$, both approximations converge to H and δ. These approximations allow the algorithm to compute a global minimizer, as described in [17].

Parameterizing the descent direction by an artificial time $t \geq 0$, the equation in $\phi(t, x, y)$ (with $\phi(0, x, y) = \phi_0(x, y)$ defining the initial contour) is

$$\frac{\partial \phi}{\partial t} = \delta(\phi)[\mu \cdot div(\frac{\nabla \phi}{|\nabla \phi|}) - \lambda^+(u_0 - c^+)^2 + \lambda^-(u_0 - c^-)^2] = 0 \tag{10}$$

where $t \in (0, \infty), (x, y) \in \Omega$.

3 Results

The experimental evaluation of the proposed image segmentation method was realized using 31 breast, 29 testicular and 24 thyroid medical US images containing hypo-echoic pathological findings. The acquired digital images had a resolution of 256×256 pixels and 256 gray-level depth.

A special purpose software suite was developed in Microsoft Visual C++ for the implementation of the two methods described in Section 2. Both methods were applied on each of the available US images. For the purposes of our study we adopted the image intensity as the supervising feature for the contour evolution, to enable the detection of hypo-echoic regions associated with pathological findings. The model constants used in the experiments are $\lambda^+ = 5$, $\lambda^- = 5$, $\mu = 650$ and $a = 10^{-13}$.

An expert radiologist manually delineated the pathological findings to enable comparisons with the deformable models. As a measure of similarity between the area inside the model delineation *A* and the area inside the expert's delineation *B* we use the overlap value [3]:

$$i = \frac{A \cap B}{A \cup B} \tag{11}$$

For a perfect matching between the two delineations *A* and *B*, *i* is expected to be equal to 1.

The average differences Δi of the overlap values and the corresponding standard deviations are presented in Table 1 ($\Delta i = i_1 - i_2$, where i_1 measures the overlap obtained using the proposed model and i_2 measures the overlap obtained using the original model [17]). The results show that in all cases the proposed deformable model achieves higher overlap values and thus more accurate image segmentation. Moreover, with the proposed model the convergence was reached in 10% less algorithm iterations on average compared to the original model, and in approximately 8.5% speedup in terms of absolute execution time.

Table 1. Average differences of the overlap values $\Delta i = i_1 - i_2$ and the corresponding standard deviations for the three types of medical US images

US Images	Δi Average	Δi Standard Deviation
Breast	7.8	5.3
Testicular	7.6	5.4
Thyroid	8.1	5.9

Indicative delineations performed by using the proposed model are illustrated in Fig. 1 for the case of a breast abscess (Fig. 1a), for the case of a testicular seminoma (Fig. 1b) and a thyroid nodule (Fig.2c).

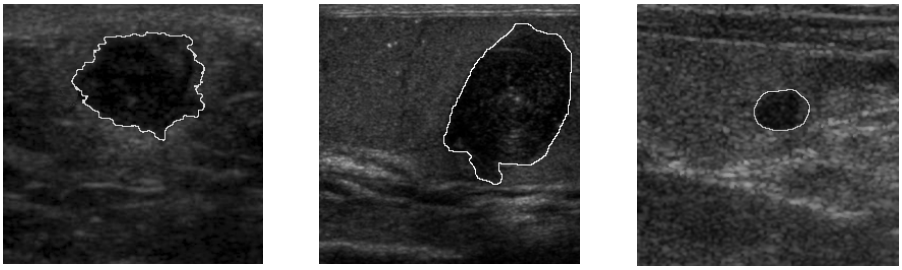

(a) (b) (c)

Fig. 1. Three example medical US images containing hypo-echoic pathological findings delineated by the proposed model: (a) breast abscess, (b) testicular seminoma and (c) thyroid nodule.

4 Conclusions

We have proposed a novel deformable model for medical US image segmentation derived from the model posed in [17] and applied it for the detection of hypo-echoic pathological findings. The results of its application on breast, testicular and thyroid US images lead to the following conclusions:

i) In all cases it has lead to accurate delineation of the pathological findings.
ii) The proposed model achieves more accurate delineations when compared to the original model [17].

iii) It converges faster than the original model [17].

Future perspectives of this work include the embedment of textural features to supervise contour evolution, which could enable the detection of iso-echoic pathological findings.

Acknowledgment

We would like to acknowledge Dr. N. Dimitropoulos, Radiologist, for the provision of part of the medical US images used in the experiments. This work was partially funded by the National and Kapodistrian University of Athens, Special Account of Research Grants.

References

1. Adams, R., Bischof, L.: Seeded Region Growing. IEEE Trans. on Pattern Analysis and Machine Intell. 16 (6) (1994) 641–647
2. Pohle, R., Toennies, K.: Segmentation of Medical Images using Adaptive Region Growing. Proc. SPIE (Medical Imaging 2001), 4322 (2001) 1337–1346
3. Hao, X., Bruce, C., Pislaru, C., Greenleaf, J.F.: A Novel Region Growing Method for segmenting ultrasound images. IEEE International Ultrasonics Symposium, Oct. 2000.
4. Boukerroui, D., Basset, O., Guerin, N., Baskurt, A.: Multiresolution Texture Based Adaptive Clustering Algorithm for Breast Lesion Segmentation. Eur. J. Ultrasound. 8 (1998) 135–144.
5. Thomas, J.G., Peters, R.A., Jeanty, P.: Automatic Segmentation of Ultrasound Images using Morphological Operators, IEEE Trans. On Med. Imaging, vol. 10, pp. 180-186, 1991.
6. Zimmer, Y., Tepper, R., Akselrod, S.: A Two-Dimensional Extension of Minimum Cross Entropy Thresholding for the Segmentation of Ultrasound Images. Ultrasound in Medicine and Biology. 22 (1996) 1183–1190
7. Fan, L., Braden, G.A., Herrington, D.M.: Nonlinear Wavelet Filter for Intracoronary Ultrasound Images. Proc. of 23rd Annual Meeting on Computers in Cardiology. (1996) 41–44
8. Kotropoulos, C., Pittas, I.: Segmentations of Ultrasonic Images Using Support Vector Machines. Pattern Recognition Letters. 24 (2003) 715–727 .
9. Heckman, T.: Searching for Contours. Proc. of SPIE. (1996) 223-232.
10. Solaiman, B., Roux, C., Rangayyan, R.M., Pipelier, F., Hillion, A.: Fuzzy Edge Evaluation in Ultrasound Endosonographic Images. Proc. of the 1996 Canadian Conference on Electrical and Computer Engineering (1996) 335-338.
11. Chen, C.M., Lu, H.H.S., Hsiao, A.T.: A Dual-Snake Model of High Penetrability for Ultrasound Image Boundary Extraction. Ultrasound in Med. and Biol. 27 (12) (2001) 1651–1665
12. Plissiti, M.E., Fotiadis, D.I., Michalis, L.K., Bozios, G.E.: An Automated Method for Lumen and Media-Adventitia Border Detection in a Sequence of IVUS Frames. IEEE Trans. on Inf. Tec. in Biomedicine. 8 (2) (2004) 131–141
13. Chang, R.F., Wu, W.J., Tseng, C.C., Chen, D.R., Moon, W.K.: 3-D Snake for US in Margin Evaluation for Malignant Breast Tumor Excision Using Mammotome. IEEE Trans. on Inf. Tec. in Biomedicine. 7 (3) (2003) 197–201
14. Angelini, E., Holmes, J., Laine, A.: Segmentation of RT3D Ultrasound with Implicit Deformable Models Without Gradients. Proc. of ISPA. 2 (2003) 711-716

15. Honigmann, D., Ruisz, J., Pottmann, H.: Fast Model Based Segmentation of Ultrasound Data using an Active Image. Proc. IEEE Int. Symp. on Biomedical Imaging (2002) 225–228
16. Lin, N., Yu, W., Duncan, J.S: Combinative Multi-scale Level Set Framework for Echocardiographic Image Segmentation. Medical Image Analysis. 7 (2003) 529–537
17. Chan, T.F., Vesse, L.A.: Active Contours Without Edges. IEEE Trans. Image Processing. 7 (2001) 266–277
18. Mumford, D., Shah, J.: Optimal Approximation by Piecewise Smooth Functions and Associated Variational Problems. Commun. Pure Appl. Math. 42 (1989) 577–685
19. Morrel, J.M., Solimini, S.: Segmentation of Images by Variational Methods: A Constructive Approach. Revista Matematica Universidad Computense de Madrid. 1 (1988) 169–182